

Supporting Information for:

Chemistry through Cocrystals: Pressure-Induced Polymerization of $C_2H_2 \cdot C_6H_6$ to an Extended Crystalline Hydrocarbon

Matthew D. Ward^a, Haw-Tyng Huang^b, Li Zhu^a, Arani Biswas^c, Dmitry Popov^f, John V. Badding^{b,c,d,e} and Timothy A. Strobel^{*a}

^aGeophysical Laboratory, Carnegie Institution of Washington, 5251 Broad Branch Road Northwest, Washington, D.C. 20015, United States

^bDepartment of Materials Science and Engineering, ^cDepartment of Chemistry, ^dMaterials Research Institute, and ^eDepartment of Physics, Pennsylvania State University, University Park, Pennsylvania 16802, United States

^fHigh Pressure Collaborative Access Team (HPCAT), Geophysical Laboratory, Carnegie Institution of Washington, Argonne, Illinois 60439, United States

Equation of state for $C_2H_2 \cdot C_6H_6$

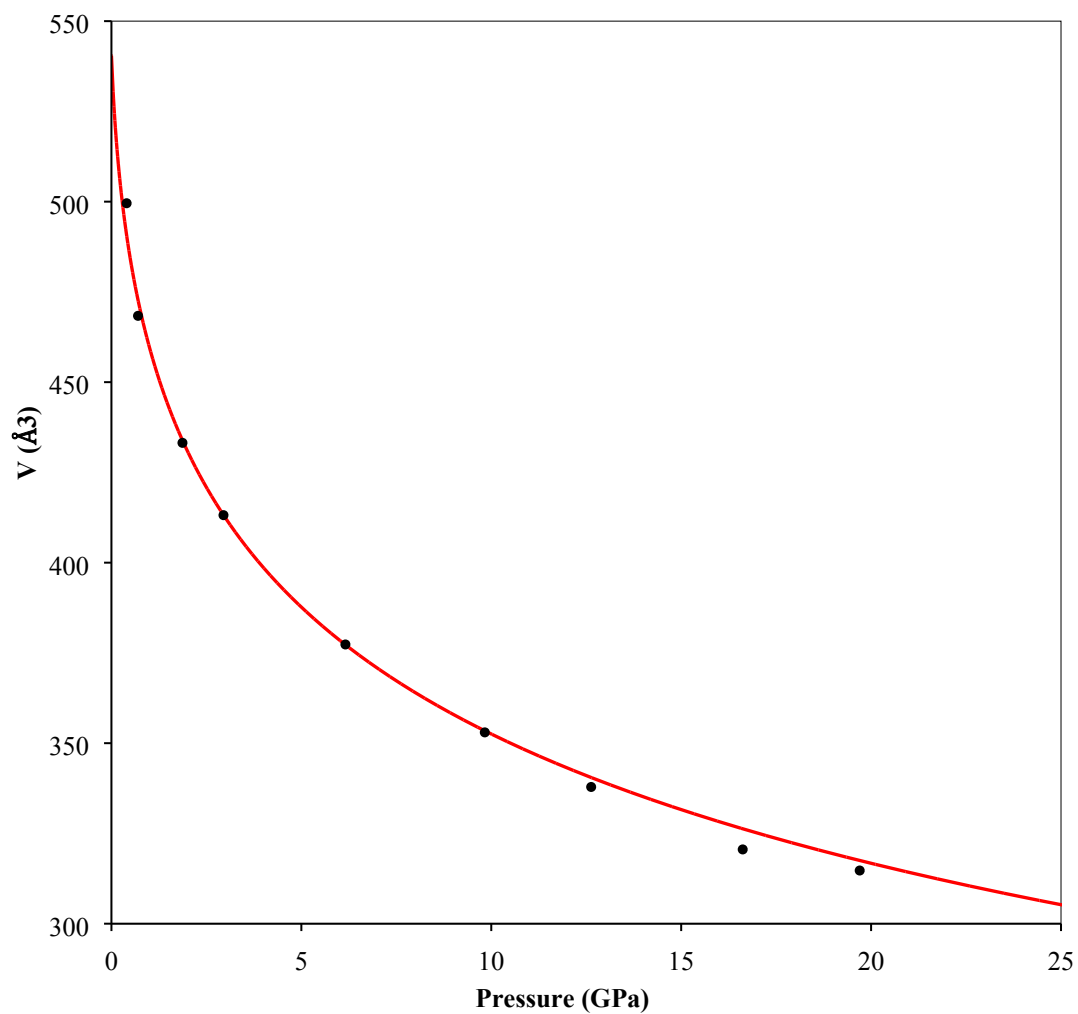


Fig. S1 Pressure dependence of unit cell volume for $C_2H_2 \cdot C_6H_6$.^{1, 2} The third order Birch-Murnaghan equation of state parameters are as follows: $V_0 = 540.43(1) \text{ \AA}^3$, $K_0 = 2.0(4) \text{ GPa}$, $K_0' = 17(4)$

Experimental vs. theoretical Raman for $C_2H_2 \cdot C_6H_6$

Table S1 Calculated and experimental Raman modes for $C_2H_2 \cdot C_6H_6$ at 5 GPa.

Vibrational Mode	Mode Character/Symmetry	Theoretical Raman Shift (cm^{-1})	Experimental Raman Shift (cm^{-1})
ν_1	C–H Stretch, C_2H_2 / A_{1g}	3341.44	3327.1
ν_2	C–H Stretch, C_6H_6 / A_{1g}	3102.03	3102.3
ν_3	$C \equiv C$ Stretch, C_2H_2 / A_{1g}	1995.17	1975.5
ν_4	Ring Stretch, C_6H_6 / A_{1g}	1034.29	1015.2
ν_5	C–H Stretch, C_6H_6 / E_g	3083.53	3093.7
ν_6	Ring Stretch, C_6H_6 / E_g	1605.90	1602.2
ν_7	C–H Bend, C_6H_6 / E_g	1153.93	1195.3
ν_8	C–H Bend, C_6H_6 / E_g	830.09	–
ν_9	C–H Bend, C_2H_2 / E_g	618.43	647.0
ν_{10}	Ring Deform, C_6H_6 / E_g	594.20	616.9
	Lattice Mode / E_g	186.25	234.6
	Lattice Mode / E_g	88.61	161.9

At 5 GPa, lattice, ν_5 , ν_7 , ν_9 , and ν_{10} modes are observed at higher frequencies in the experimental spectrum than the calculation, while the experimental ν_1 , ν_3 and ν_4 modes are observed at slightly lower frequency (See Fig. 2 in the main text). The ν_2 and ν_6 modes overlap well with calculated spectrum. All of the observed modes can be compared to previous experimental observations for molecular acetylene and benzene. In particular, it is important to note the position of the $C \equiv C$ stretch for acetylene at $\sim 1990 \text{ cm}^{-1}$ (Fig. S2, panel 6 and Fig. S3). This is the most intense mode for acetylene and, as acetylene is known to polymerize to polyacetylene at ~ 3.5 GPa, will be a primary indicator of the formation of the acetylene-benzene cocrystal.

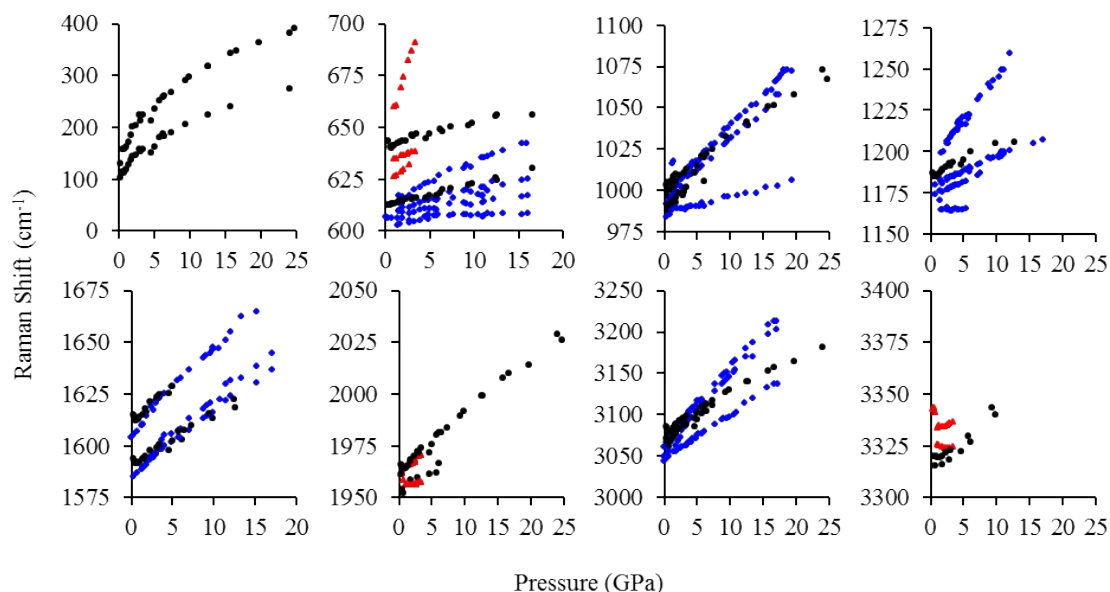


Fig. S2 Pressure dependence of the observed Raman modes in $C_2H_2 \cdot C_6H_6$. Separate panels indicate different frequency regions. $C_2H_2 \cdot C_6H_6$, acetylene, and benzene are represented by black, red, and blue markers respectively. Data points for $C_2H_2 \cdot C_6H_6$ are collated from multiple loadings with small variances in pressure calibration. Data for acetylene and benzene are incorporated from Aoki et. al. and Thiéry and Léger.^{3,4}

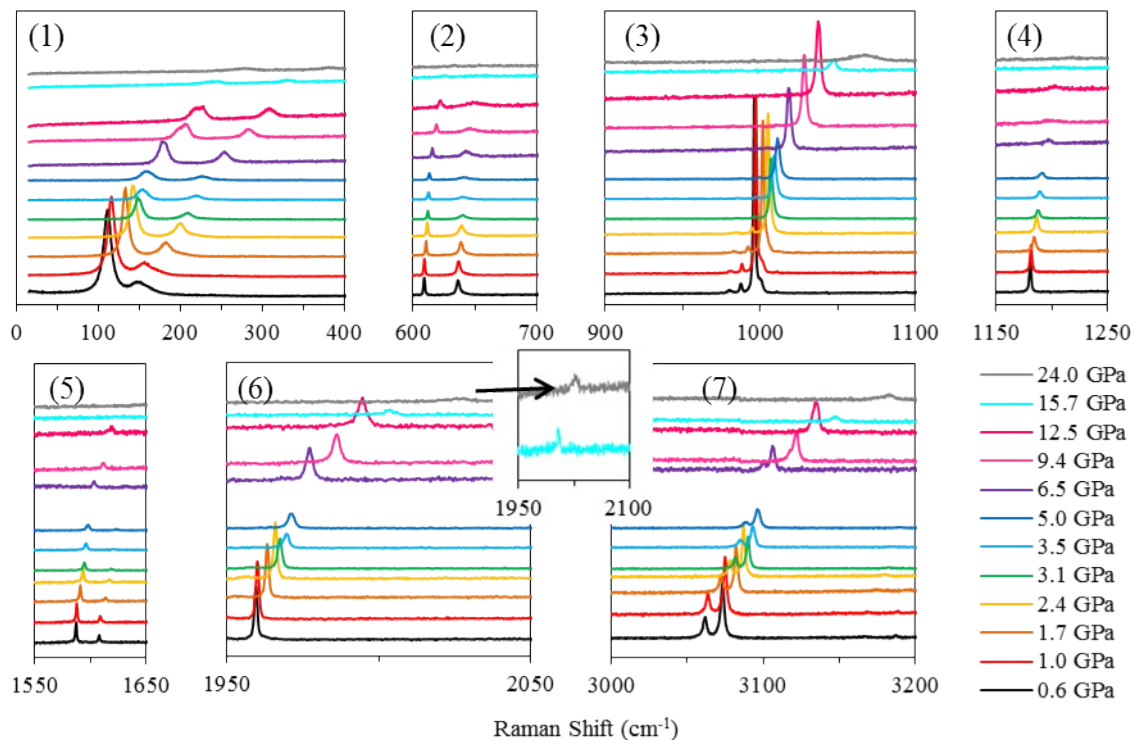


Fig. S3 Raman spectra of $C_2H_2 \cdot C_6H_6$ from 0.58 GPa to 23.99 GPa. The fluorescence background has been subtracted for spectra from 6.46 GPa to 23.99 GPa. Panel numbers correspond to the same frequency regions as in Fig. S2. Panel 6 shows a zoomed in view of the $C \equiv C$ stretching mode at higher pressures.

FT-IR for $C_2H_2 \cdot C_6H_6$

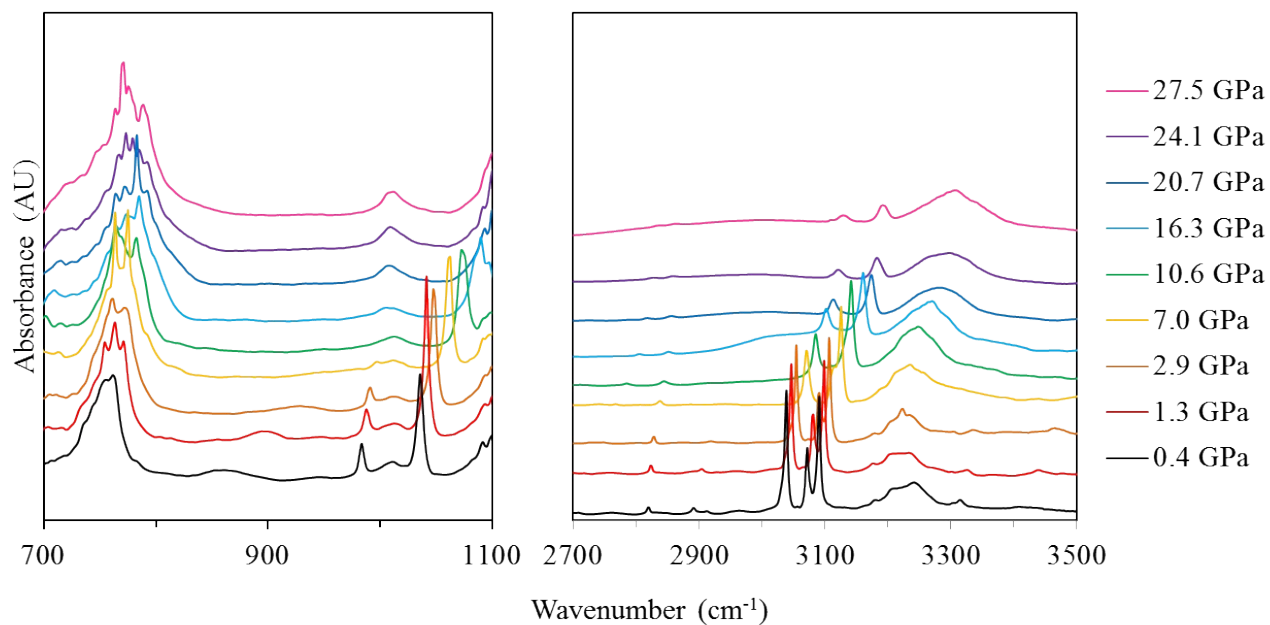


Fig. S4 FT-IR spectra of $C_2H_2 \cdot C_6H_6$ from 0.40 GPa to 27.45 GPa.

For the FT-IR measurements on $C_2H_2 \cdot C_6H_6$ (Fig. S4), the low-energy detection limit is 700 cm^{-1} and absorption from the diamonds occurs from $1100\text{--}1600\text{ cm}^{-1}$, limiting the number of observable modes. Orthorhombic acetylene at 1.1 GPa was previously shown to exhibit three peaks within the present region of interest at 762 , 3236 , and 3401.1 cm^{-1} corresponding to C–C–H antisymmetric deformation, C–H antisymmetric stretch, and C–H symmetric stretch, respectively.⁵ FT-IR studies of benzene under pressure have shown three C–H stretch bands above 3000 cm^{-1} , two C–H bending bands at $\sim 975\text{ cm}^{-1}$ and $\sim 1030\text{ cm}^{-1}$ and a ring deformation band at $\sim 1000\text{ cm}^{-1}$.^{6,7}

The cocrystal in the present study exhibits the expected FT-IR modes for both molecular acetylene and benzene with some expected shifting and/or broadening of the bands. In particular, the acetylene C–C–H antisymmetric deformation and C–H antisymmetric stretch at 770 cm^{-1} and 3223 cm^{-1} are significantly broader and weaker than in molecular acetylene. It is important to note that the mode at 3223 cm^{-1} becomes relatively more intense and less broad as pressure increases. It is also notable that this band is observable even at the highest measured pressure (27.5 GPa), again indicating that acetylene is trapped in the cocrystal and that no chemistry has occurred between acetylene and benzene at this pressure.

XPS Analysis of Polymerized $C_2H_2 \cdot C_6H_6$

The XPS spectra of the recovered $C_2H_2 \cdot C_6H_6$ sample are shown in Fig. S5. The survey spectrum in Fig. S5(A) shows that the recovered material is composed mostly of carbon with some oxygen (17 at%) present from surface oxidation occurring during recovery. Only trace oxygen was detected in the bulk sample after surface cleaning. Notably, there's also a small amount of silicon (2 at%) present on the surface. Therefore, a small portion of the O1s peak intensity can be attributed to contamination from SiO_x particles from the adhesive material used to hold the gasket in place during DAC loading.

The C1s envelopes from XPS before and after sputtering are shown in Figs. 5(B,C). Notably, the C1s envelope in Fig. S5(B) can be fit with two primary components centered at 284.4 and 281.7 eV along with a smaller component attributed to C=O surface oxidation at 287.5 eV. The larger of the two C1s peaks has been calibrated to be centered at 284.4 eV based on charge reference to the Pt $4f_{7/2}$ band at 71.2 eV. In this case, the splitting of the observed peaks centered at 284.4 eV and 281.7 eV is unusually large (2.7 eV) for a pure carbon material and assignment of components under the C1s envelope is not particularly straightforward. Typically, the sp^3 peak is shifted $\sim 1\text{ eV}$ higher than the sp^2 peak, which is usually assigned to 284.3 eV for graphite.^{8,9} However, some authors also concluded that the C1s binding energy of diamond should be located at a lower binding energy position (283.8 eV) with respect to graphite.⁸ Samples that contain large amounts of fullerenic carbon have been noted to have shifts larger than 1 eV to the lower binding energy side with respect to graphite.⁹

As a result, the bands of interest located at 284.4 eV and 281.7 eV can't be easily assigned according to hybridization of carbon atoms or curvature of the carbon structure. In this case, the peak at 284.4 eV has been assigned as indicative of hydrocarbon (CH_x) including both sp^2 and sp^3 hybridized carbon.¹⁰ The peak at 281.7 eV is attributed to fullerenic carbon and/or highly oriented polyacetylene-like carbon chains, which can be corroborated by the HRTEM images and EELS spectra (Figs. S7,S8). Based upon the qualitative observation from the FT-IR spectrum of the recovered sample, which suggests that the C–H stretching region is primarily from sp^3 hybridized carbon, the CH_x band at 284.4 eV is considered to be largely sp^3 hybridized, although the possibility of incorporation of sp^2 carbon cannot be excluded. In this case, quantitative analysis of the XPS C1s envelope with the peak at 284.4 eV as sp^3 and the peak at 281.7 eV as sp^2 hybridized carbon results in an assignment of 85% sp^3 /10.6% sp^2 before surface cleaning (Fig. S5(B)) and 70.5% sp^3 /29.5% sp^2 after surface cleaning (Fig. S5(C)). This quantization should be considered as an upper bound for the amount of sp^3 carbon in the recovered sample as the peak at 284.4 eV will have some contribution from sp^2 carbon.

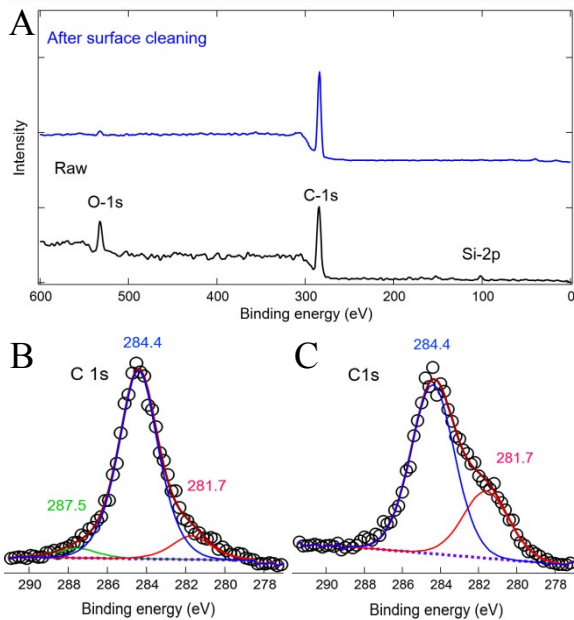


Fig. S5 (A) XPS survey spectrum of recovered $C_2H_2 \cdot C_6H_6$ after decompression from 30 GPa before and after surface cleaning. (B) C1s envelope before surface cleaning. (C) C1s envelope after surface cleaning.

Polyacetylene observed in XPS

The delocalization of the outer shell electron densities of carbon gives rise to an unusually large shift toward the lower binding energy side.¹¹ Although the typical binding energy of pristine polyacetylene is located at 283.7 eV, it can be decreased further after doping as the electron density increases along the chain.^{11, 12} Given that pressure-induced polymerized acetylene should have the π electrons of starting acetylene molecules in close proximity due to the pressure; it is possible that the pressure history could give rise to a similar binding energy lowering effect as doping.

Plasmon Loss Features

Band 2 centered at 308 eV in the plasmon region (Fig. S6) can be attributed to the surface plasmon of diamond. However, the contribution from the amorphous carbon plasmon peak which occurs at 310 eV cannot be excluded. In addition, band 1, which occurs at 301 eV is significantly higher in energy than the 298 eV of the interband transition of diamond. The origin of this band is unknown, although it agrees with observations of CVD diamond thin film.

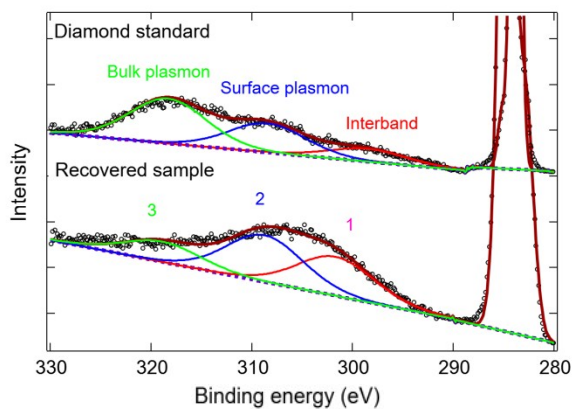


Fig. S6 The plasmon loss feature of the recovered $C_2H_2 \cdot C_6H_6$ shows a prominent diamond bulk plasmon hump centered at 320 eV (band 3). Compared with a type Ia diamond standard, the diamond content presented of the recovered material is assessed to be 29 at%.

TEM SAED Analysis of Recovered Polyacetylene

Excess acetylene from loading presents itself as particles of highly oriented polyacetylene (HOPA) along with few-layered graphene (Fig. S7(A)). The inset FFT further demonstrates the presence of two discrete phases as the graphitic layers display lower crystallinity indicated by the diffuse halo. The HOPA is beam sensitive and starts to transform at a critical dose rate of $180 \text{ e}/\text{\AA}^2 \text{ sec}$. Therefore, atomic resolution HRTEM images are not achievable with the limited amount of dose that can be applied. However, with the help of Fourier-filtered HRTEM image, it is possible to unambiguously identify the presence of highly crystalline trans-polyacetylene by the wavy striations as shown in Fig. S7(B). The asymmetric FFT pattern (Fig. S7(B) inset) is indexed to the $\langle 1-30 \rangle$ zone of trans-polyacetylene. In addition, the streaking arc in the FFT pattern with a d -spacing value of $\sim 2.0 \text{ \AA}$ is consistent with the $\{310\}$ plane reflection of trans-polyacetylene. The streaking and smeared intensities suggests that the HOPA is not a defect-free single-crystal, but likely to have multiple twins and stacking faults.

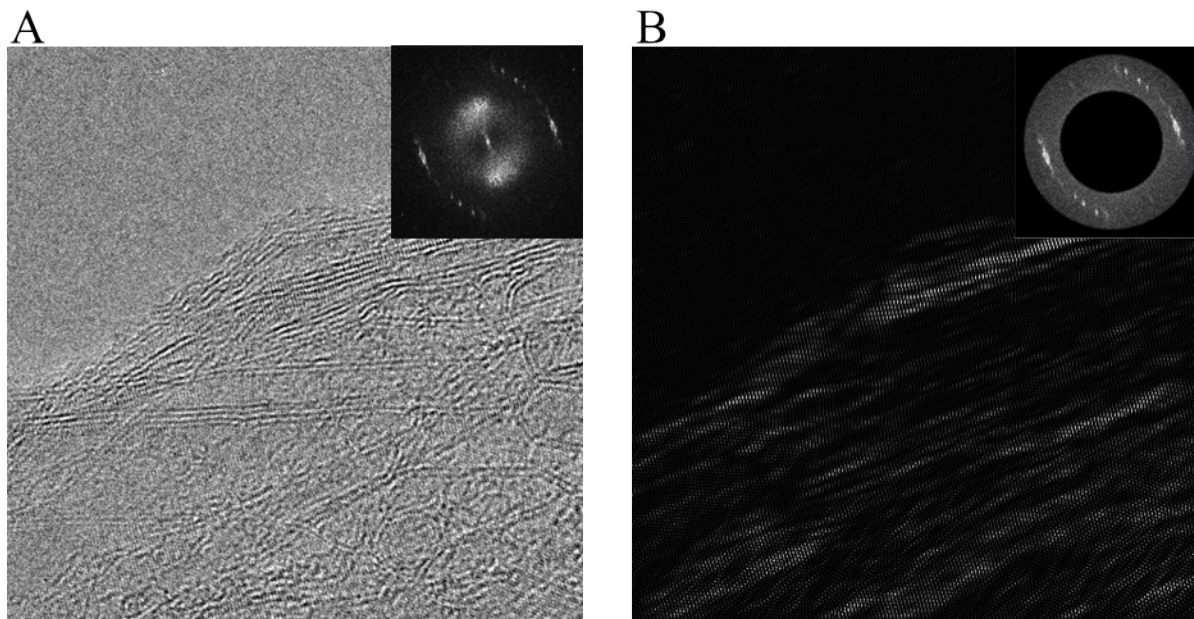


Fig. S7 (A) HRTEM image and the inset FFT show the presence of highly-oriented polyacetylene (HOPA) along with few-layer graphene. (B) The Fourier filtered image accentuates the presence of trans-polyacetylene as wavy striations. The asymmetric FFT pattern may be indexed to the $\langle 1-30 \rangle$ zone of trans-polyacetylene.

The dose dependent EELS further confirms the presence of HOPA as shown in Fig. S8(A). Before reaching the critical dose, the EELS spectra shows a more prominent $1s$ to π^* peak and less intense $1s$ to $2p^*$ peak when compared to the isotropic $100\% sp^2$ carbon nano-onion standard. This occurs when the electron beam is incident at an angle perpendicular to the delocalized p_z orbitals.

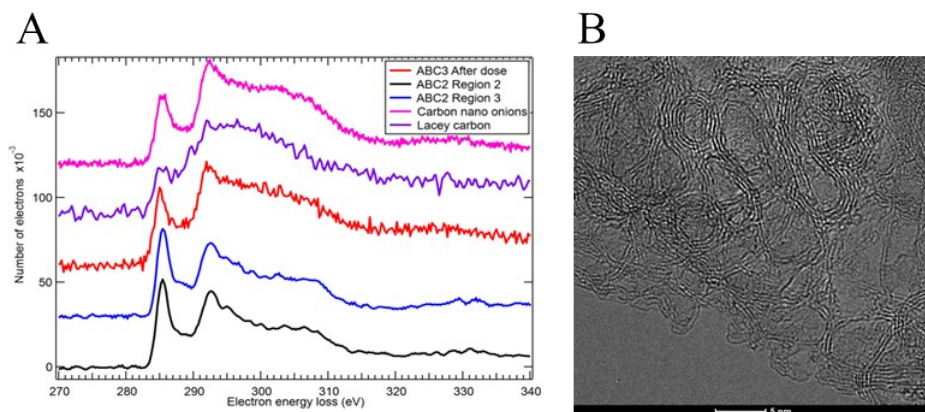


Fig. S8 (A) Low dose EELS spectra shows the evolution of the $1s$ to π^* (C=C) and $1s$ to σ^* (C-C) peaks before and after high dose electron radiation. The typical EELS spectrum of carbon nano-onions is used as a $100\% sp^2$ carbon standard. The transformed sample is quantified to contain $97 \text{ at}\%$ sp^2 carbon. (B) HRTEM image of the transformed polyacetylene indicates formation of spherical and elliptical onion like carbon nanostructures after high dose electron radiation.

The EELS intensity agrees with previous studies on anisotropic carbon materials with delocalized π electrons^{13,14} and serves as unequivocal support for the presence of a highly directional delocalized π electron system observed in the XPS. Moreover, the relatively small interplanar spacing of {310} (~ 2.0 Å), compared to the interplanar spacing of pristine polyacetylene (~ 2.1 Å),^{15,16} indicates that the pressure-induced polymerization has led to a denser packing of polymer chains, resulting in a lower C 1s binding energy.

The origin of this HOPA phase is attributed to excess acetylene which polymerizes at ~ 3.5 GPa. After initial polymerization, the polyacetylene experiences a "mechanical annealing process" when compressed to 30 GPa and results in HOPA. Recently, a mechanical annealing method which led to the stress-induced crystallization of Au nanoparticles has been reported.¹⁷ It was demonstrated that the pressure related term in the Gibbs free energy ($dG=dH-TdS+PdV$) may have an influence on nanoparticle self-assembly. It is possible that a similar effect can be applied to a pressure-induced polymerization. This may offer new opportunities to tune the structure/charge density and the related properties of polymeric materials. Further investigation is still in progress.

Interestingly, HOPA transforms under electron radiation and forms spherical multi-wall nano-onion like structures (Fig. S8(B)). This agrees with previous reports on the pyrolysis of polyacetylene thin films.^{18,19} The formation mechanism of nano-graphite from a polyacetylene crystal during the dehydrogenation and carbonization process has also been proposed.¹⁹ This could explain the presence of few-layered graphene as the moderate annealing in the DAC could have similar effect.

EDS Analysis of Recovered $C_2H_2 \cdot C_6H_6$

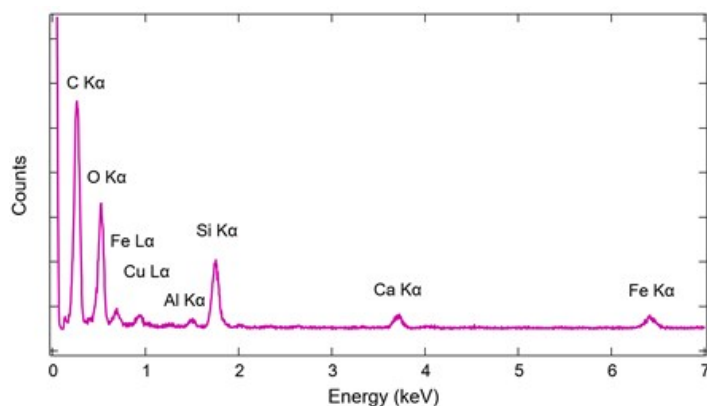


Fig. S9 EDS spectrum of the recovered $C_2H_2 \cdot C_6H_6$ material on a silicon monoxide supporting film TEM grid.

The EDS spectrum for recovered $C_2H_2 \cdot C_6H_6$ is shown in Fig. S9. The peaks corresponding to Si K α and O K α are attributed to the SiO grid. The peaks for Cu L α and Fe K α are attributed to stray X-rays which hit the Cu grid and pole piece of the microscope. There are also some minor impurities such as alumina (ruby) and calcite which can be incorporated during the DAC synthesis process. However, the relative intensities of these possible contaminants compared to those for Cu L α and Fe K α are weak and may also be attributed to stray X-rays. In addition, the XPS survey of the recovered material shows that the sample is composed primarily of carbon with a small amount of surface oxidation and a small amount of Si, possibly from the adhesive used to hold the gasket in place. Thus, the sample is considered to be composed almost entirely of carbon and the other peaks are the result of instrumental artifacts or stray X-rays.

EELS Analysis of Recovered $C_2H_2 \cdot C_6H_6$

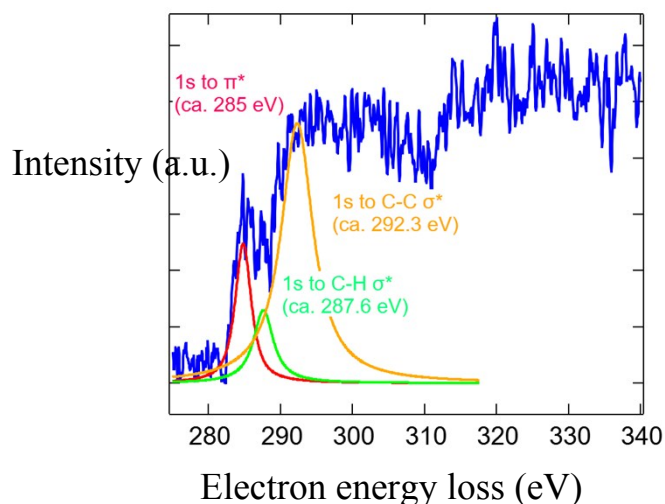


Fig. S10 Low dose EELS spectrum of the recovered $C_2H_2 \cdot C_6H_6$ material and deconvolution of the carbon core-excitation peaks. The $1s/\sigma^*$ (C-H) transition can be clearly resolved with a controlled accumulated dose of less than $1,000 \text{ e}/\text{\AA}^2$.

Molecular Dynamics of $C_2H_2 \cdot C_6H_6$

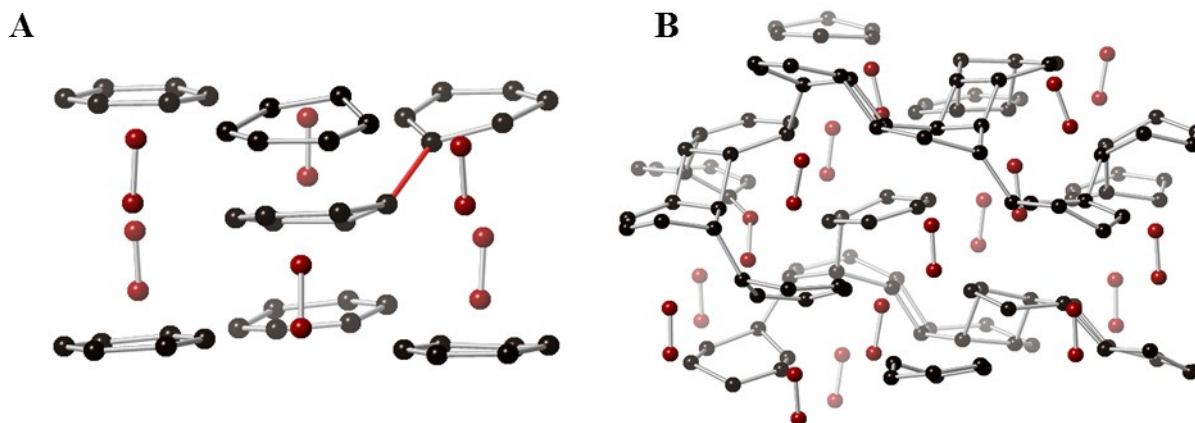


Fig. S11 Molecular dynamics simulations of $C_2H_2 \cdot C_6H_6$ at various pressure/temperature conditions. Carbon atoms from benzene and acetylene are represented as black and dark red spheres, respectively. Hydrogen atoms have been omitted for clarity. (A) Molecular dynamics simulation at 40 GPa/500 K and 3 ps. Initial C-C bond formation (Red bond, distance = 1.554 \AA) occurs between carbon atoms from adjacent benzene molecules. (B) Molecular dynamics simulation at 100 GPa/1000 K and 0.5 ps. As polymerization continues, bond formation continues to occur between carbon atoms from adjacent benzene molecules resulting in four-membered cyclobutane rings with many benzene molecules participating in multiple 2+2 cycloadditions. Only one new bond is observed with carbon atoms from acetylene. In all simulations, a significant driving force (pressure and/or temperature) was required to observe rare event reactions on computationally reasonable time scales.

References:

1. J. Angel Ross, M. Alvaro and J. Gonzalez-Platas, *Journal*, 2014, **229**, 405.
2. J. Gonzalez-Platas, M. Alvaro, F. Nestola and R. Angel, *Journal of Applied Crystallography*, 2016, **49**, 1377-1382.
3. M. M. Thiéry and J. M. Léger, *The Journal of Chemical Physics*, 1988, **89**, 4255-4271.
4. K. Aoki, Y. Kakudate, S. Usuba, M. Yoshida, K. Tanaka and S. Fujiwara, *The Journal of Chemical Physics*, 1988, **88**, 4565-4568.
5. M. Sakashita, H. Yamawaki and K. Aoki, *The Journal of Physical Chemistry*, 1996, **100**, 9943-9947.
6. L. Ciabini, M. Santoro, R. Bini and V. Schettino, *The Journal of Chemical Physics*, 2002, **116**, 2928-2935.
7. P. Pruzan, J. C. Chervin, M. M. Thiéry, J. P. Itié, J. M. Besson, J. P. Forgerit and M. Revault, *The Journal of Chemical Physics*, 1990, **92**, 6910-6915.
8. G. Speranza and N. Laidani, *Diamond and Related Materials*, 2004, **13**, 451-458.
9. J. T. Titantah and D. Lamoen, *Diamond and Related Materials*, 2007, **16**, 581-588.
10. W. Cheng, L.-T. Weng, Y. Li, A. Lau, C. K. Chan and C.-M. Chan, *Aerosol Science and Technology*, 2013, **47**, 1118-1124.
11. H.-M. Wu and S.-A. Chen, *Synthetic Metals*, 1988, **26**, 225-236.
12. H.-M. Wu and S.-A. Chen, *Synthetic Metals*, 1987, **20**, 169-183.
13. R. D. Leapman, P. L. Fejes and J. Silcox, *Physical Review B*, 1983, **28**, 2361-2373.
14. M. M. Disko, O. L. Krivanek and P. Rez, *Physical Review B*, 1982, **25**, 4252-4255.
15. K. Shimamura, F. E. Karasz, J. A. Hirsch and J. C. W. Chien, *Die Makromolekulare Chemie, Rapid Communications*, 1981, **2**, 473-480.
16. G. Perego, G. Lugli, U. Pedretti and M. Cesari, *Die Makromolekulare Chemie*, 1988, **189**, 2657-2669.
17. H. Wu, Z. Wang and H. Fan, *Journal of the American Chemical Society*, 2014, **136**, 7634-7636.
18. H. Gu, R. Zheng, X. Zhang and B. Xu, *Advanced Materials*, 2004, **16**, 1356-1359.
19. A. Goto, M. Kyotani, K. Tsugawa, G. Piao, K. Akagi, C. Yamaguchi, H. Matsui and Y. Koga, *Carbon*, 2003, **41**, 131-138.